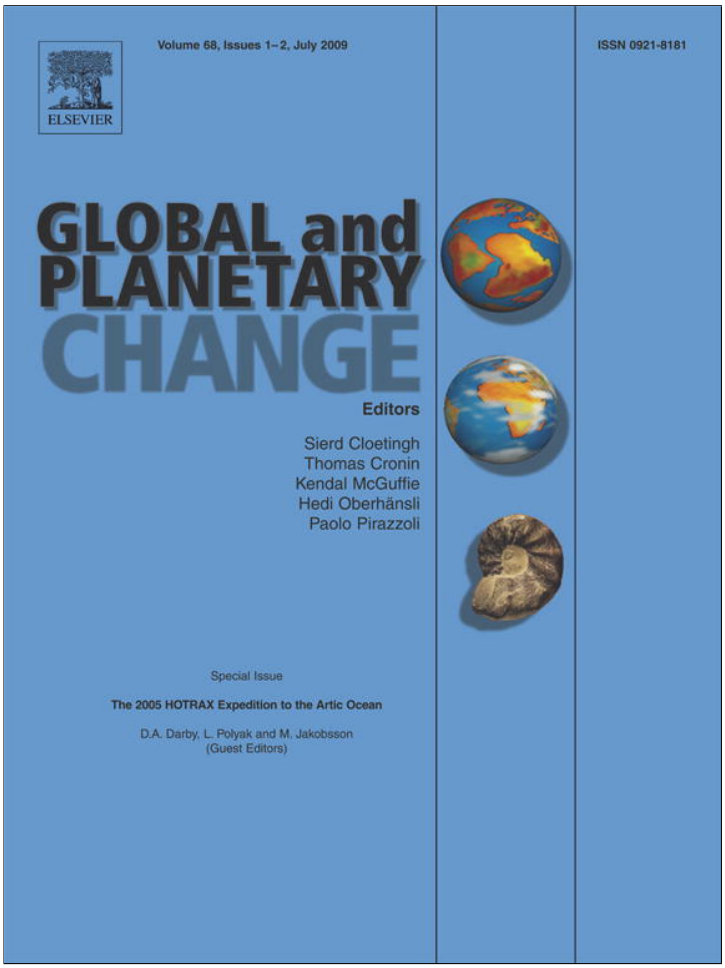

Global and Planetary Change 68 (2009) 18–29

Contents lists available at ScienceDirect

Global and Planetary Change

journal homepage: www.elsevier.com/locate/gloplacha

Sediment record from the western Arctic Ocean with an improved Late Quaternary age resolution: HOTRAX core HLY0503-8JPC, Mendeleev Ridge

Ruth E. Adler [a,b,*], Leonid Polyak [a], Joseph D. Ortiz [c], Darrell S. Kaufman [d], James E.T. Channell [e], Chuang Xuan [e], Andréa G. Grottoli [b], Emma Sellén [f], Kevin A. Crawford [a,b]

[a] Byrd Polar Research Center, Ohio State University, Columbus, Ohio 43210, USA
[b] School of Earth Sciences, Ohio State University, Columbus, Ohio 43210, USA
[c] Department of Geology, Kent State University, Kent, Ohio 44242, USA
[d] Department of Geological Sciences, University of Florida, Gainesville, FL 32611, USA
[e] Department of Geology, Northern Arizona University, Flagstaff AZ 86011, USA
[f] Department of Geology and Geochemistry, Stockholm University, Stockholm, Sweden

ARTICLE INFO

Article history:
Accepted 25 March 2009
Available online 3 May 2009

Keywords:
Arctic Ocean
Mendeleev Ridge
sediment stratigraphy
Late Quaternary
glaciations
last interglacial

ABSTRACT

Sediment core HLY0503-8JPC raised by the HOTRAX'05 expedition from the Mendeleev Ridge was analyzed for multiple lithological, paleontological, and stable-isotopic proxies to reconstruct paleoceanographic conditions in the western Arctic Ocean during the Late Quaternary. The core, extensively sampled in the upper 5 m, reveals pronounced changes in sedimentary environments during the ca. 250 kyr interval encompassing Marine Isotopic Stages (MIS) 1 to 7. An estimated average resolution of 500 yr/sample, at least for the last glacial cycle including the last interglacial, provides more detail than seen in other sedimentary records from the western Arctic Ocean. The age control is provided by ^{14}C and amino acid racemization measurements on planktonic foraminifers and correlations with the stratigraphy developed for the central Lomonosov Ridge and with glacial events at the Eurasian Arctic margin. Cyclic variations in lithology combined with foraminiferal abundance and stable-isotopic composition indicate profound changes in hydrographic and depositional environments between interglacial-type and glacial-type periods apparently reflecting a combination of 100-kyr and precessional time scales. This periodicity is complicated by abrupt iceberg- and/or meltwater-discharge events with variable (Laurentide vs. Eurasian) provenance. The proxy record from the interval identified as the last interglacial (MIS 5e), which may aid in understanding the future state of the Arctic Ocean, indicates low ice conditions and possibly enhanced stratification of the water column.

1. Introduction

Current dramatic changes in the Arctic climatic and oceanic system, including notably the rapid retreat in sea-ice cover (e.g., Comiso et al., 2008) necessitate a thorough investigation of paleoclimatic conditions. These data will help us to understand the long-term Arctic variability and to constrain prognostic models for future climate using analogs from the past, especially from warm periods such as Quaternary interglacials. This requires sedimentary records with an adequate age resolution to be investigated from key sites across the Arctic Ocean for a comprehensive representation of paleoceanographic environments. One of the important areas for characterizing paleocirculation in the western Arctic Ocean is the Mendeleev Ridge, where sedimentation at different time periods could be affected by either the Transpolar Drift or the Beaufort Gyre, the two major modern Arctic circulation features (Fig. 1). In 2005, the Healy–Oden TransArctic Expedition (HOTRAX) collected sediment cores across the Arctic Ocean (Darby et al., 2005) including core HLY0503-8JPC that showed relatively elevated thickness of lithologic units in its upper part, indicating potentially high sedimentation rates. This, combined with good preservation of calcareous fossils in the upper part of the Mendeleev Ridge stratigraphy (Polyak, 1986; Poore et al., 1999; Polyak et al., 2004), makes HLY0503-8JPC well suited for a detailed representation of sedimentary environments in the western Arctic Ocean in the recent geological past. This paper focuses on the upper part of the Quaternary stratigraphy, up to MIS 7, which has been shown to contain the best preserved calcareous fossils in many Arctic cores (e.g., Jakobsson et al., 2001; Spielhagen et al., 2004).

In this study we use various sedimentary proxies such as sediment color, density, sand content, distribution of planktonic and benthic foraminifers, and stable oxygen and carbon isotopic composition of planktonic foraminiferal calcite to reconstruct Late Quaternary paleoceanographic environments on the Mendeleev Ridge. Biomarker distribution is discussed in a concurrent paper (Yamamoto and Polyak,

* Corresponding author. Current address: Department of Geological Sciences, Case Western Reserve University, Cleveland, OH 44106, USA. Fax: +1 216 368 3691.
E-mail address: rea47@case.edu (R.E. Adler).

0921-8181/$ – see front matter © 2009 Elsevier B.V. All rights reserved.
doi:10.1016/j.gloplacha.2009.03.026

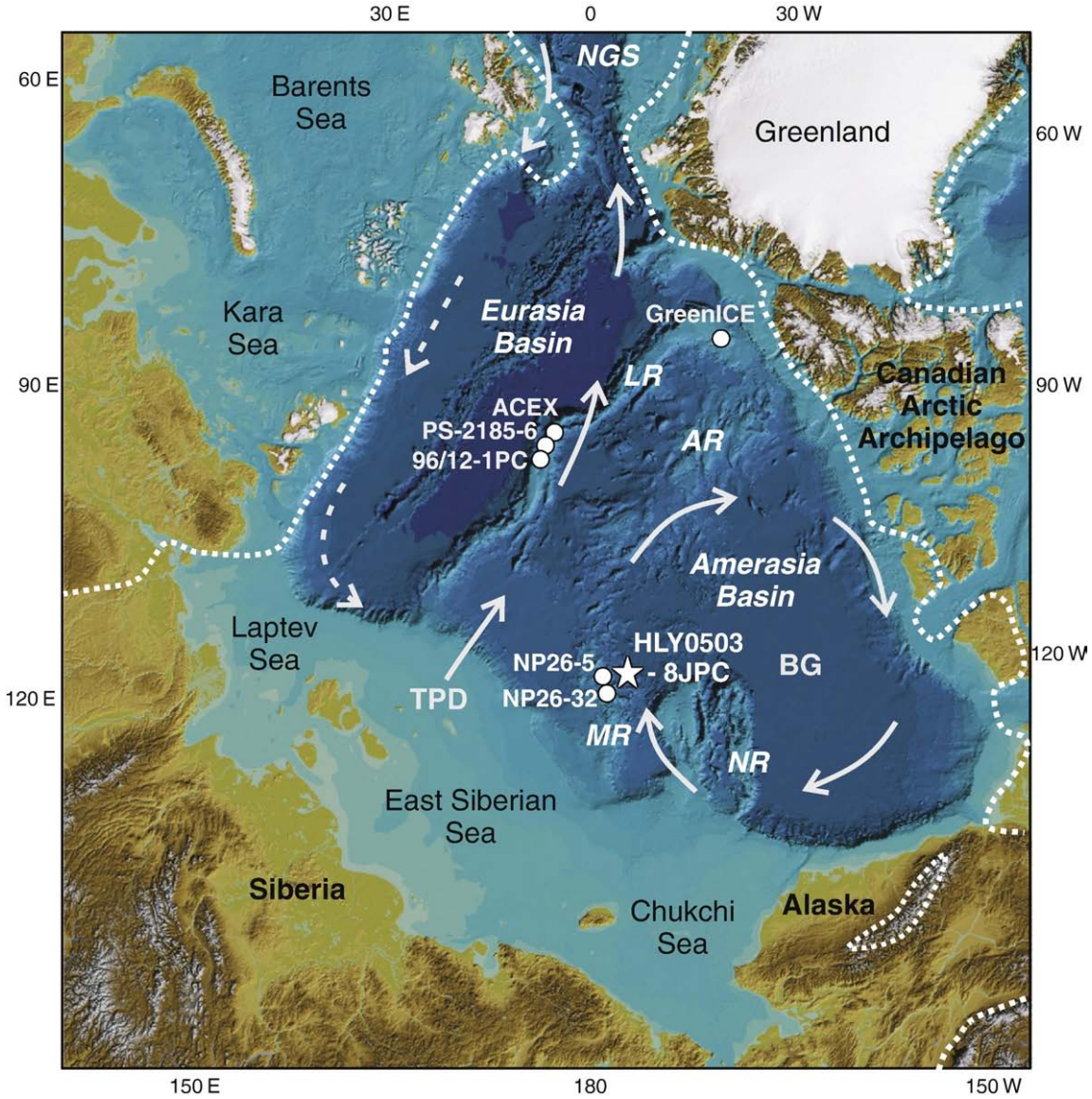

Fig. 1. Index map of the Arctic Ocean showing core sites used in the paper: star for HLY0503-8JPC, circles for other cores. LR, MR, AR, and NR are Lomonosov, Mendeleev, Alpha, and Northwind ridges, respectively; NGS — Norwegian–Greenland Sea. Arrows show major circulation features: Beaufort Gyre (BG), Transpolar Drift (TPD), and Atlantic water inflow (dashed arrows for subsurface current). Base map is the International Bathymetric Chart of the Arctic Ocean (IBCAO-2) (Jakobsson et al., 2008a). Dotted lines show the maximal limit of Late Pleistocene glaciations in North America and Eurasia (Dyke et al., 2002; Svendsen et al., 2004).

2009-this issue). The age of sediment is constrained by AMS ^{14}C and amino acid racemization (AAR) values generated on planktonic foraminiferal tests along with correlation to the stratigraphy developed for the central Lomonosov Ridge (Jakobsson et al., 2000, 2001; Spielhagen et al., 2004; O'Regan et al., 2008) and with glacial stratigraphy at the Eurasian Arctic margin (Svendsen et al., 2004; Larsen et al., 2006). We especially aim to gain a better understanding of the Arctic paleoceanography during warm, low-ice intervals, notably during the last interglacial, potentially a close analog for climatic conditions of the near future (Otto-Bliesner et al., 2006).

2. Oceanographic and sedimentary background

The Arctic Ocean is characterized by a strongly stratified water column featuring low-salinity surface water with a large runoff component, intermediate layers including the cold halocline, warm (>0 °C) and saline water advected from the North Atlantic, and cold-saline bottom waters (e.g., Aagaard et al., 1985). The two main surface, wind-driven circulation systems are the clockwise Beaufort Gyre in the western Arctic and the Transpolar Drift that carries water and ice from the Siberian margin to the Norwegian-Greenland Sea. The front between these systems is generally located west of the Mendeleev Ridge, but changes its position depending on atmospheric conditions (Rigor et al., 2002). Intermediate water levels may contain counter-clockwise boundary currents carrying water mostly of Atlantic and Siberian shelf origin as well as eddies of different scales extending into the basin interior (Aagaard et al., 1985; Rudels et al., 2004).

Productivity in the central Arctic Ocean is generally low and is primarily controlled by sea-ice conditions and levels of insolation (e.g., Gosselin et al., 1997). The short vegetation period results in a pulsed annual delivery of organic material to the sea floor. Benthic populations are more abundant and diverse at shallower depths near the margins and on submarine ridges, possibly due to the advection of food from the shelves in intermediate waters (Clough et al., 1997).

Sedimentation in the Arctic Ocean is strongly controlled by the dispersal of sediment by drifting ice — mostly sea ice in modern conditions, but with numerous icebergs during glacial periods (Darby et al., 2006 and references therein). Fine sediment can also be

transported by subsurface and deep-water currents, especially near the margins and over the ridges (Hunkins et al., 1969; Fahl and Nöthig, 2007). The biogenic sediment component, mostly represented by calcareous planktonic foraminiferal tests, is generally low, but can reach over 10% of the sediment mass in some stratigraphic intervals.

During Quaternary times, the nearly landlocked Arctic Ocean experienced profound changes in hydrographic, biological, and sedimentary conditions related to sea-level fluctuations and repeated formation of large continental ice sheets at the Arctic periphery. These fluctuations are recorded in various components of the sedimentary record such as in the physical properties of sediment, fossil assemblages, and their chemical composition. The sedimentary record of the last two glacial cycles shows dramatic variations in sediment characteristics; this cyclicity appears to be more muted, yet recognizable in older Pleistocene deposits (Jakobsson et al., 2000; O'Regan et al., 2008). Investigation of these sedimentary variations is key for understanding how the Arctic Ocean system operates on glacial-interglacial time scales.

Interpretation of Arctic sedimentary records is hampered by stratigraphic problems related to the lack of close analogs for the Arctic system, generally low sedimentation rates, and limited biogenic proxies due to low productivity and dissolution of fossil material. The most up-to-date age model was developed on sediment cores from the central part of the Lomonosov Ridge, the site of the first deep-drilling record from the central Arctic (Jakobsson et al., 2000, 2001; Backman et al., 2004; O'Regan et al., 2008). The younger part of this stratigraphy is generally consistent with the long-term Cenozoic record (Cronin et al., 2008; O'Regan et al., 2008) and has been shown to be suitable for wide trans-Arctic correlations (Spielhagen et al., 2004). However, this stratigraphy still has considerable open questions, and its correlation to other areas of the Arctic Ocean, especially those with different sedimentation rates, is not straightforward (Sellen et al., 2008). The development of stratigraphic schemes for various sedimentary areas across the Arctic Ocean is critical for the interpretation of the paleoclimatic evolution of the Arctic.

3. Materials and methods

Core HLY0503 (Healy, 2005, Leg 3)-8JPC was raised from the base of the eastern flank of the Mendeleev Ridge (79°35.6′ N, 172°30.1′ W, 2792 mwd, total length ~12 m) (Fig. 1). The whole core was logged shipboard on a Geotek Multi-Sensor Core Logger for the gamma-ray density, compressional p-wave velocity, and magnetic susceptibility at 1 cm increments. The split core was described for lithology, photographed, x-rayed, logged at 1-cm resolution for Diffuse Spectral Reflectance in the visible spectra using a Minolta CM-2600d spectrophotometer, and u-channeled for paleomagnetic analyses. The core was then continuously subsampled at 1 cm intervals to 500 cm. Freeze-dried samples were wet-sieved on a 63 μm mesh, and >63 μm fractions were oven dried at 65 °C, weighed for coarse grain size, and sieved at larger meshes for foraminiferal counts and general microscopic examination of the coarse sediment. Size fraction >150 μm in all samples was used for total planktonic and benthic foraminiferal abundance counts; in addition, planktonic foraminifers were identified to the species level in >75-μm fractions at sparser intervals (every 4 cm down to 280 cm core depth and at 4 to 12 cm further down-core). Because sand-sized sediment in some intervals includes considerable amounts of foraminiferal tests or manganese micronodules, >63 μm sediment weight was compared to bulk density for estimates of detrital inputs (Fig. 2). Bulk density typically approximates the content of detrital silt and sand (e.g., Weber et al., 1997), and the initial results of fine (<63 μm) particle size analysis in the upper 1 m of HLY0503-8JPC confirm a close relationship between bulk density and silt content (D. Darby, pers. comm., 2009). The distribution of clasts coarser than sand, reaching up to several cm in diameter, was additionally evaluated using x-radiographs.

Simultaneous measurements of $\delta^{18}O$ and $\delta^{13}C$ were run on tests of adult (encrusted) planktonic foraminifer *Neogloboquadrina pachyderma* (sinistral), hereafter Nps, picked from the 150–250 μm size fraction so as to minimize potential size dependent effects (e.g. Hillaire-Marcel et al., 2004). Subsamples with masses of ~85–105 μg

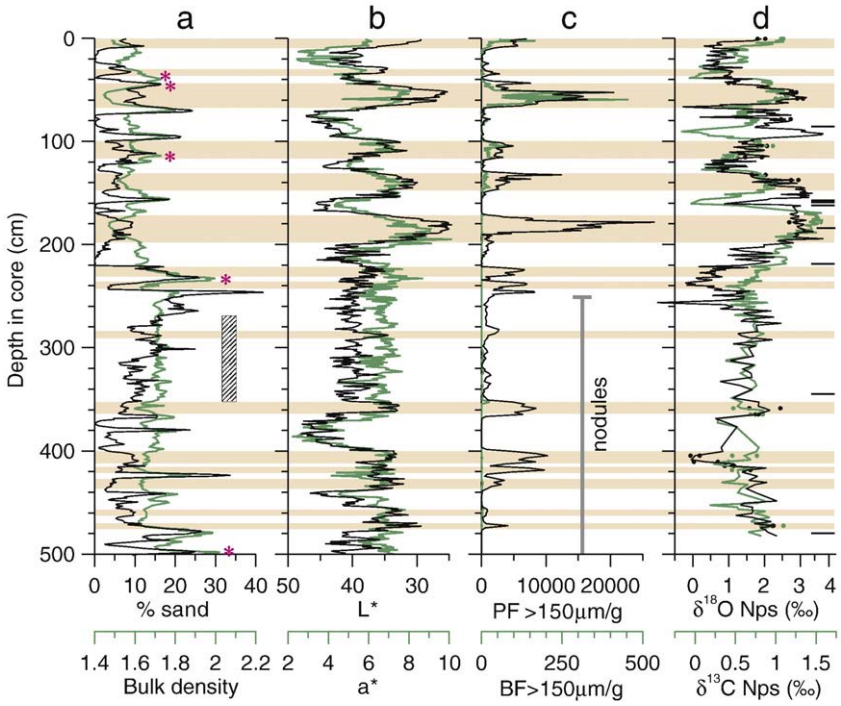

Fig. 2. Downcore distribution of proxies in HLY0503-8JPC: (a) sand content (>63 μm) and bulk density, (b) L* and a*, (c) planktonic and benthic foraminiferal numbers, (d) stable isotopes in Nps (curves show singular measurements or the average between duplicates shown by circles; rejected data points are indicated by bars on the right; $\delta^{18}O$ scale is reversed to enable a comparison with $\delta^{13}C$). Brown units are shaded; unshaded are lighter colored, grayish/yellowish units. Detrital carbonate layers are shown by stars and slump interval is indicated by a stippled bar next to (a). Fe–Mn micronodule occurrence range is shown next to (c).

Table 1
Radiocarbon ages.

Lab ID[a]	HLY0503 core ID	Depth in core (cm)	^{14}C age (yr BP)	1σ (±)	Calibrated age (yr BP)[b]	1σ range (±)
AA74470	8JPC	0–1	3981	46	3984	72
UCIAMS 53933	8JPC	3–4	8530	25	9167	58
AA74471	8JPC	7–8	9314	76	10,151	103
AA74472	8JPC	14–15	8940	63	9608	79
AA74473	8JPC	24–25	9917	50	10,857	127
UCIAMS 53934	8JPC	25–26	11,445	30	12,953	42
AA77887	8JPC	32–33	36.250	730	41,118	681
AA74475	8JPC	34–35	32,480	470	37,467	502
AA74476	8JPC	43–44	38,660	980	43,218	863
AA74477	8JPC	48–49	30,950	400	35,926	404
AA74478	8JPC	52–53	>43,300	na	na	na
AA74479	8JPC	56–57	37,820	880	42,493	781
AA74480	8JPC	62–63	40,500	1300	44,816	1149

[a] Samples were analyzed by AMS at the NSF Radiocarbon Facility, University of Arizona (AA) or University of California, Irvine (UCIAMS).
[b] Holocene ages are median probability ages based on calibration using CALIB v 5.0.2 (http://calib.qub.ac.uk/calib/); older ages were calibrated using the Fairbanks0107 program [Fairbanks et al., 2005]. No ΔR was applied.

(ca. 12 tests), but as little as ~40 μg (5 tests) when more were not available, were analyzed for $\delta^{18}O$ ($\delta^{18}O$ = permil deviation of ^{18}O:^{16}O relative to Vienna Peedee Belemnite Limestone standard (V-PDB)) and $\delta^{13}C$ ($\delta^{13}C$ = permil deviation of ^{13}C:^{12}C relative to V-PDB) using an automated Carbonate Kiel device coupled to a Finnigan Delta IV Plus stable isotope ratio mass spectrometer in the Stable Isotope Biogeochemistry Laboratory at The Ohio State University. Samples were acidified under vacuum with 100% ortho-phosphoric acid, the resulting CO_2 was cryogenically purified, and delivered to the mass spectrometer. Approximately 10% of all samples were run in duplicate and showed reproducible results. The standard deviation of repeated measurements of an internal standard was ±0.023‰ for $\delta^{13}C$ and ±0.045‰ for $\delta^{18}O$. Results with low intensity and high standard deviation as well as solitary outliers, typically with suspiciously low values, were rejected (<3% rejection of all measurements) (Fig. 2).

Accelerator Mass Spectrometry (AMS) ^{14}C ages were measured on non pretreated planktonic foraminiferal samples of 5–8 mg from abundance maxima in the upper ~70 cm of the core at the Arizona AMS Lab (Table 1). Nps samples from the same intervals and abundance maxima further down-core were analyzed for amino acid racemization (AAR) (Kaufman et al., 2008) with a focus on aspartic and glutamic acids; aspartic acid is especially abundant in foraminifer protein and racemizes at a high rate for enhanced age resolution at low ambient temperatures (Goodfriend et al., 1996). Each sample was analyzed in two to nine subsamples (average = 5), each composed of 3 to 10 Nps tests (average = 8). Details of the analytical procedure are provided in Kaufman et al. (2008).

Natural remanent magnetization (NRM) was measured at 1 cm spacing on u-channel samples after alternating field (AF) demagnetization at 14 steps in the 10–100 mT peak field range. Component magnetization directions were determined using the standard 3-D least squares method (Kirschvink, 1980).

4. Results

4.1. Lithostratigraphy

The sediment of the core consists of conspicuous alternating dark brown (10YR 3/3 to 4/4 in the Munsell scale) and lighter colored, yellowish or grayish (mostly 10YR 5/4 to 2.5Y 5/4) units of 5–30 cm thickness (Figs. 2 and 3a). Brown units have been shown to represent interglacial or interstadial periods, and grayish units — glacial or stadial and deglacial periods in cores from the Mendeleev Ridge (Polyak, 1986; Poore et al., 1999; Polyak et al., 2004) and across the central Arctic Ocean at sites where sedimentation rates are high enough so that individual units are discernible (e.g., Poore et al., 1993, 1994; Phillips and Grantz, 1997; Jakobsson et al., 2000; O'Regan et al., 2008). Brown units are characterized by low L* and high a* values (sediment color lightness and 'redness', respectively), low bulk densities, low to moderate amounts of detrital sand with occasional coarser grains, elevated content of biogenic component predominantly comprised of foraminifera, and generally enriched $\delta^{18}O$ and $\delta^{13}C$ compositions in Nps (Fig. 2). The upper boundary of each brown unit is typically distinct while the lower boundary has evidence of bioturbational disturbance. Grayish/yellowish units have characteristically high L* and low a* values, low biogenic accumulation, and generally depleted $\delta^{18}O$ and $\delta^{13}C$ compositions with some pronounced $\delta^{18}O$ minima. The sand and coarser grain distribution in grayish units is heterogeneous and includes: (1) fine grained intervals with very low sand content, but elevated bulk density indicative of considerable silt contribution, and (2) distinct sand and some coarser grain spikes, typically near the top and/or bottom of the unit. This pattern is best exemplified by the grayish unit between ~70 to 100 cm that contains a fine-grained interval bound by two sand spikes.

The interval between 270–350 cm differs from the rest of the core by distinct flow-type sedimentary structures such as convoluted bedding and the lack of normal stratification (Fig. 3b). We consider this sediment to represent a slump or gravity-flow deposit (e.g., Carter, 1975; Middleton and Hampton, 1976) and hereafter refer to it as slump.

A consistent lithological feature in the core is light-colored, whitish to pinkish sediment (10YR 6/4 to 7.5YR 7/3, but pure color is difficult to determine due to patchy occurrence) with abundant coarse debris composed of detrital carbonates (see also Polyak et al., 2009-this issue). Typically this sediment occurs in bioturbated layers a few mm

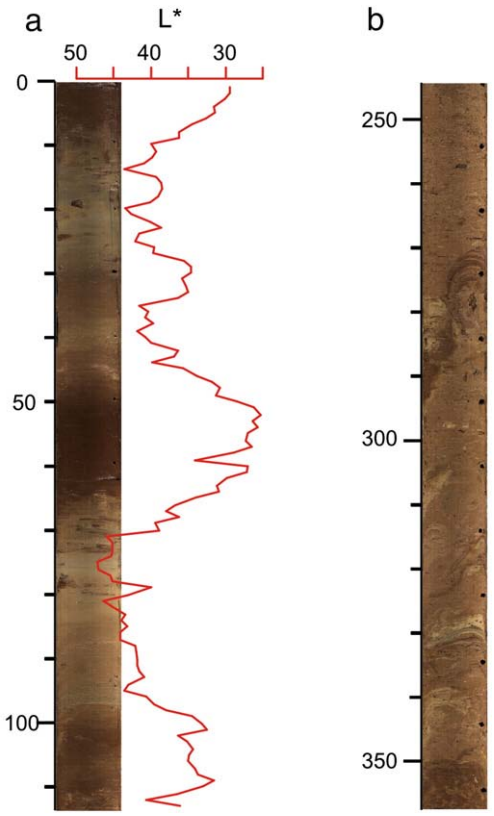

Fig. 3. Photographic fragments of HLY0503-8JPC that exemplify (a) normal stratification, with brown/gray interlamination approximated by L*, and (b) interval with gravity-flow sedimentary structures between 270 to 350 cm.

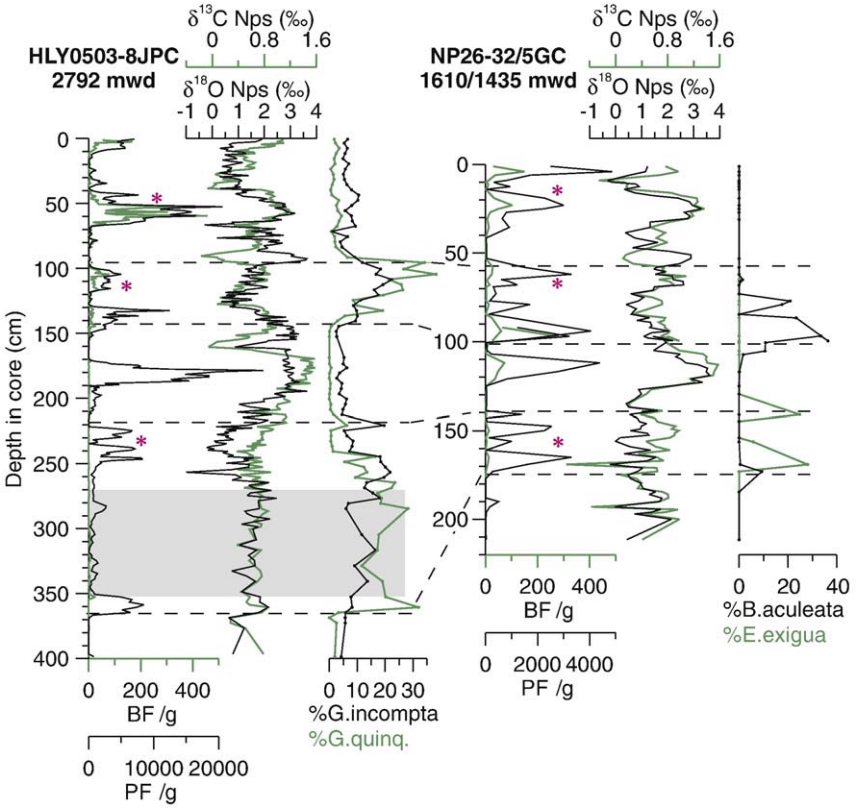

Fig. 4. Correlation between HLY0503-8JPC and NP26 record (Polyak et al., 2004): planktonic and benthic foraminiferal numbers (>150 μm), stable isotopes in Nps ($\delta^{18}O$ is plotted as in Fig. 2), subpolar planktonic foraminifers *N. incompta* and *T. quinqueloba* in HLY0503-8JPC, and benthic foraminifers *B. aculeata* and *E. exigua* in NP26. Dashed lines bound intervals with elevated numbers of low-ice foraminiferal indicators; major detrital carbonate layers are shown by stars; slump interval in HLY0503-8JPC is shaded. Note different scales for depth in cores and for planktonic foraminiferal numbers.

to several cm thick near the top or bottom of brown units and is accompanied by a marked decrease in foraminiferal abundance. The most conspicuous whitish or pinkish layers occur at ~45, 115, 230, and 500 cm, but this sediment can be also found in small patches, especially in the upper part of the core. Similar layers have been identified in cores across the western Arctic Ocean as detrital carbonates, predominantly dolomites of the Canadian Arctic (Laurentide) provenance (Darby, 1971; Bischof et al., 1996; Phillips and Grantz, 2001).

4.2. Biostratigraphy

The biogenic component is abundant in the sand fraction in brown beds and is predominated by planktonic, then benthic foraminifers, with lesser numbers of other faunal remnants composed of calcite (ostracodes, echinoid spines) and silica (sponge spicules). Grayish beds exhibit only scarce faunal remains that mostly co-occur with brown inclusions in lighter-colored sediment indicating either bioturbation from the above brown units or transitional environments.

Planktonic foraminifers in the >150 μm size fraction are almost entirely represented by the sinistral morphotype of *N. pachyderma*. They reach very high abundances up to >20 000 per gram sediment in brown units in the upper 2.5 m of the core. These numbers are considerably higher than in nearby cores from shallower areas of the Mendeleev Ridge exemplified by cores NP26-32 and 5 (Fig. 4) (Polyak et al., 2004). The reason for that is not clear and may be related to a more restricted pelagic sedimentation on the crest of the ridge due to higher current activity. In contrast, benthic microfauna in many intervals is less abundant and diverse in HLY0503-8JPC, probably due to a lower food supply with increasing water depth.

In contrast to the large size fractions, the study of planktonic foraminifers <150 μm revealed significant numbers of subpolar species *Turborotalita quinqueloba* and *Neogloboquadrina incompta*, commonly referred to as *N. pachyderma* dextral (counts of *N. incompta* may include some amount of actual *N. pachyderma* dextral). These foraminifers are especially abundant in two HLY0503-8JPC intervals, between 95–150 cm and 220–350 cm, where they comprise up to 50% of the total planktonic assemblage. Similar subpolar planktonic peaks, composed mostly of *T. quinqueloba*, have been demonstrated for the GreenICE core north of Greenland, the only well-constrained stratigraphic record from the central Arctic Ocean where planktonic foraminifers have been identified in small size fractions (Nørgaard-Pedersen et al., 2007). These peaks, indicative of low-ice conditions, were attributed to the last interglacial (MIS 5e) and a later relatively warm interval, MIS 5a. Unlike GreenICE data, some intervals in HLY0503-8JPC contain high numbers of *N. incompta*, which is a true subpolar species in comparison with *T. quinqueloba* that thrives in the frontal zones including the ice-marginal zone (Johannessen et al., 1994). Comparison of HLY0503-8JPC with NP26 data (Fig. 4) suggests that the subpolar planktonic peaks correspond to elevated contents of benthic foraminifers *Bulimina aculeata* and *Epistominella exigua*, which are not common for the modern Arctic Ocean and likely indicate low ice conditions (Ishman et al., 1996; Polyak et al., 2004).

Dissolution of calcareous tests (predominantly foraminifera) is not evident in the upper ~2.5 m of the core. Below this level calcareous foraminifers occur in smaller numbers and appear to bear signs of dissolution, which co-occurs with numerous Fe–Mn micronodules appearing below 2.5 m. This change may reflect stronger dissolution associated with diagenetic processes possibly related to variations in organic productivity and/or bottom ventilation (e.g., Glasby, 2006, and references therein). Stratigraphic correlations indicate that the lowermost foraminiferal peak at ~480 cm marks the transition to almost calcite-barren sediment across the central Arctic Ocean (e.g., Kaufman et al., 2008), likely indicating pervasive carbonate dissolution.

4.3. Stable oxygen and carbon isotopes

The $\delta^{13}C$ and $\delta^{18}O$ compositions of Nps in the Arctic represent the largely salinity-controlled $\delta^{18}O$ signal of ambient water and the $\delta^{13}C$ composition of dissolved inorganic carbon (DIC), with some offsets (e.g., Bauch et al., 1997, 2000; Volkmann and Mensch, 2001). The stable-isotopic record in HLY0503-8JPC shows pronounced variations that correspond to the brown and grayish units, with the amplitude often exceeding a 3‰ shift in $\delta^{18}O$ and near 2‰ shift in $\delta^{13}C$ (Fig. 2). Some grayish units contain very pronounced spikes in $\delta^{18}O$ depletion such as between 65 to 90 cm and at ~255 cm. Both $\delta^{13}C$ and $\delta^{18}O$ values are generally heavier in brown units and lighter in grayish units, especially in the upper two meters with the exception of an enriched $\delta^{18}O$ spike at ~90–100 cm. Below ~2 m, this stable-isotopic variability is less conspicuous; notably, with moderately depleted $\delta^{18}O$ values in the brown sediment between 220–250 cm. The overall pattern of stable-isotopic variations is consistent with other cores on the Mendeleev Ridge (Fig. 4) (Poore et al., 1999; Polyak et al., 2004) and elsewhere across the western Arctic Ocean (Spielhagen et al., 2004; Nørgaard-Pedersen et al., 2007). The $\delta^{13}C$ record shows a general co-variation with L* and planktonic foraminiferal abundance (Fig. 2), suggesting a common control on these proxies. Depletions in $\delta^{18}O$ mostly co-occur with coarse-grain peaks, which suggest a relationship with glacial meltwater discharge.

5. Age model

Age control was obtained through several independent or semi-independent proxies: AMS ^{14}C ages on the upper ~70 cm, AAR data (Kaufman et al., 2008), correlation with cores from the central Lomonosov Ridge that have an established stratigraphy extending older in time (Jakobsson et al., 2000; O'Regan et al., 2008), and correlation of glacial intervals with glaciations of the Eurasian Arctic margin (Svendsen et al., 2004; Larsen et al., 2006).

5.1. Radiocarbon ages

Multiple downcore AMS ^{14}C measurements have been commonly used for constraining the age of the upper horizons in Arctic Ocean sediment cores (Darby et al., 1997; Nørgaard-Pedersen et al., 1998; Poore et al., 1999). However, several factors complicate the use of ^{14}C stratigraphy in these sediments such as the uncertainty with reservoir ages, bioturbation of strata with low sedimentation rates, and input of detrital carbonates, potentially with associated hard water from under the Laurentide ice sheet (see more detail in Polyak et al., 2009-this issue). The latter factor may be responsible for apparently old ages around the carbonaceous layer at 35 cm.

Because of all these uncertainties, it is important to use downcore series of ^{14}C ages and check them for consistency in the analyzed core as well as in the context of age distribution in other cores from the study area. The age series in HLY0503-8JPC has some inversions, but essentially shows the same pattern as in other cores from the Mendeleev Ridge and well-dated records from other areas of the western Arctic Ocean (Darby et al., 1997; Poore et al., 1999; Polyak et al., 2004), where ^{14}C ages allow for the identification of the Holocene (upper brown unit) and pre-LGM interstadial sediments (second brown unit) with a hiatus of several thousand years between ca. 15–23 ka (see detail in Polyak et al., 2009-this issue). Post-LGM ages consistently indicate relatively high sedimentation rates during the deglaciation and early Holocene, reaching levels as high as above 20 cm/kyr around ca. 8–10 ka, and their strong subsequent decrease. The ages in the second brown unit extend to ca. 45 ka near its base, which matches the termination age of the penultimate glaciation in northern Eurasia (Svendsen et al., 2004; Larsen et al., 2006). Overall,

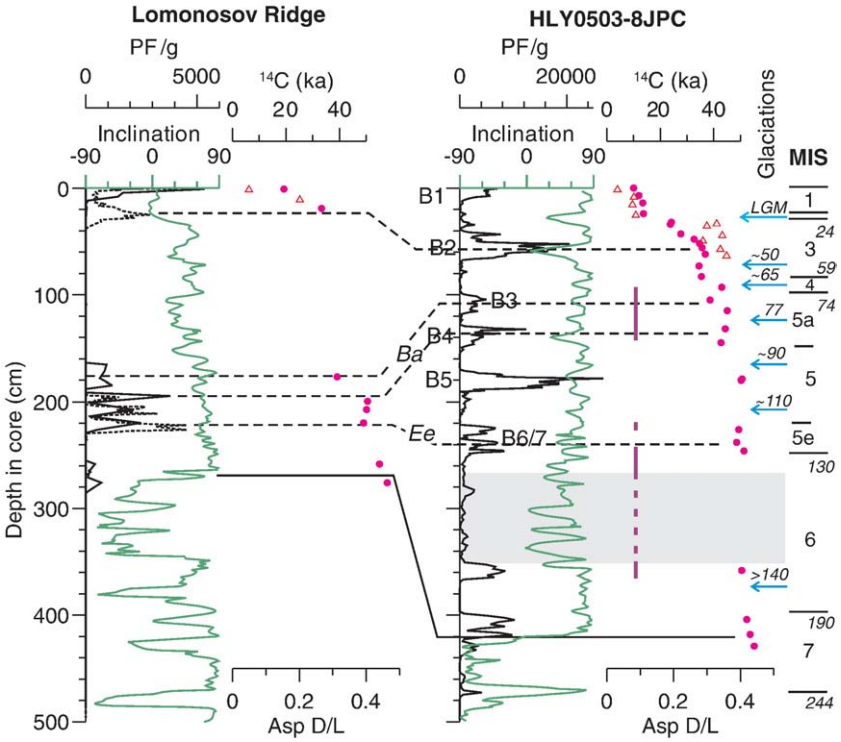

Fig. 5. Correlation between HLY0503-8JPC and the central Lomonosov Ridge stratigraphy (the latter is based on 96/12-1PC with additions spliced from PS-2185-6 and ACEX using the correlation of O'Regan et al. (2008)): paleomagnetic inclination, planktonic foraminifers (dashed curve - PS-2185-6), ^{14}C (ACEX), amino acid racemization (aspartic acid D/L values), and benthic foraminiferal correlation levels (Ba — *B. aculeata*, Ee — *E. exigua*). Triangles show calibrated ^{14}C ages, circles — amino-acid racemization (aspartic D/L) values. Vertical bars show ranges of subpolar planktonic foraminifers in HLY0503-8JPC. Correlation lines are shown for benthic foraminiferal events (dashed) and the 'inclination drop' (solid). Assignment of Marine Isotopic Stages (MIS) is based on the Lomonosov Ridge age model and refined by the distribution of subpolar foraminifers; MIS ages (Martinson et al., 1987) are shown in italics. Arrows to the left of MIS show correlation to Eurasian glaciations (approximate ages shown in italics). Slump interval between 270 to 350 cm is shaded. Note different scales for planktonic foraminiferal curves.

despite the uncertainties potentially as large as a few thousand years, the observed ^{14}C age distribution is regionally consistent and meaningful in the broad paleogeographic context.

5.2. Amino acid racemization

The extent of AAR was measured by analyzing the ratio of D- to L-enantiomers in Nps tests from 26 levels in HLY0503-8JPC along with samples from several other cores from the central Arctic Ocean (Kaufman et al., 2008). To convert D/L values to sample age, the rate of AAR was first calibrated for aspartic and glutamic acids using ^{14}C ages and correlations with the global MIS via the stratigraphy developed for the central Lomonosov Ridge (Jakobsson et al., 2000; O'Regan et al., 2008). Although the AAR ages depend on the calibration based on other age controls, the D/L values themselves provide an independent means for correlating Late Quaternary stratigraphic sequences across the Arctic Ocean. The AAR age model developed on the central Arctic cores is applicable to about 150 ka with realistic age uncertainties of about ±15% (Kaufman et al., 2008).

5.3. Stratigraphic correlations

Core HLY0503-8JPC has been compared to cores from the central Lomonosov Ridge (96/12-1PC, PS-2185-6, and ACEX) that presently constitute the best-constrained age model for the central Arctic Ocean (Jakobsson et al., 2000, 2001; Spielhagen et al., 2004; O'Regan et al., 2008; Cronin et al., 2008). The correlation illustrated on Fig. 5 is based on paleomagnetic inclination, planktonic foraminiferal abundance, the occurrence of specific benthic foraminiferal species, AAR data, and ^{14}C ages in the top part of the stratigraphy. In addition, lithological parameters such as bulk density, grain size, and spectral reflectance data have a similar cyclic pattern at both sites, although with some geographic differences. For example, glacial units on the Lomonosov Ridge are typically represented by sandy sediment, where fine-grained intervals are less common than in the correlative units in the western Arctic Ocean. Preservation of carbonaceous material also differs between the sites, with much more abundant foraminifers in HLY0503-8JPC. Some foraminiferal peaks present in this core appear to be missing in cores 96/12-1PC or PS-2185-6, whereas in the ACEX record calcareous microfossils are practically absent except for the core top. Nevertheless, the corresponding interstadial intervals are revealed in the Lomonosov Ridge sediments by other parameters such as grain size and color (O'Regan et al., 2008).

In addition to cyclic variations in lithology and faunal abundance, several non-recurring features (markers) constrain the correlation. One notable marker is the change in the pattern of paleomagnetic inclination from predominantly high values to a strongly variable record with generally negative values that occurs below ~420 cm in HLY0503-8JPC (Fig. 5). This change in remanence inclination, consistently found in cores from across the Arctic Ocean apparently at the same stratigraphic level, has often been interpreted as the Bruhnes–Matuyama polarity boundary (e.g., Steuerwald et al., 1968; Jackson et al., 1985; Poore et al., 1993). In more recent papers, the same change in remanence inclinations has been interpreted as an excursion within MIS 7 (Jakobsson et al., 2000; Backman et al., 2004; Spielhagen et al., 2004; O'Regan et al., 2008). Alternating field demagnetization of the NRM for Core HLY0503-8JPC and other investigated HOTRAX cores indicated the presence of a multi-component magnetization. A relatively high coercivity magnetization component could generally be defined in the 30–80 mT peak-field range, although the peak-field range varied due to the variable influence of lower coercivity components. For this reason, the peak field range for definition of the "characteristic" component was determined individually for each measurement level. The higher coercivity component directions were accompanied by maximum angular deviation (MAD) values generally in the 0°–10° range (see Kirschvink, 1980), indicating reasonably good definition of this component. The mean inclination associated with the "characteristic" component above the 420 cm level (58°) is, however, not consistent with the expected inclination (84°) for an axial dipole field at the site, indicating that the "characteristic" magnetization directions do not represent the ambient magnetic inclination at the time of deposition. The magnetization directions are apparently perturbed by the influence of post-depositional magnetization components. From thermal experiments, these post-depositional magnetization components are partly carried by an authigenic iron oxide (possibly titanomaghemite) (Xuan et al., 2008). We believe that the changes in inclination such as at ~420 cm in HLY0503-8JPC (Fig. 5) are lithologically rather than geomagnetically controlled, and may coincide with changes in concentration of authigenic iron oxides. Despite the current uncertainties in explaining the inclination record, the apparent consistency in stratigraphic position of the 'inclination drop' (e.g., Fig. 5; see also Backman et al., 2004; Spielhagen et al., 2004; Kaufman et al., 2008) indicates that this feature is probably related to a synchronous, basin-wide change in depositional environments possibly including changes in sedimentation rates or organic matter fluxes. It is notable that this event closely coincides with the dramatic increase in carbonate dissolution so that below this level only very limited intervals in some Amerasian Basin cores contain calcareous fossils (Scott et al., 1989; Clark et al., 1990; Andreeva et al., 2007). Because the inclination record may be diagenetically disturbed, we restrain from using it for correlation with global geomagnetic events (cf. Spielhagen et al., 2004; O'Regan et al., 2008), although some of the inclination changes might represent real variations in the geomagnetic field.

Another correlation means is based on the composition of microfaunal assemblages occurring at specific stratigraphic levels (occurrence or abundance zones). Benthic faunas are especially useful for this approach due to their higher diversity in comparison with high-latitude planktonic assemblages, especially at relatively shallow water depths that receive more food than deeper basins (e.g., Clough et al., 1997). We use benthic foraminiferal and ostracode assemblages investigated in NP26 cores from the crest of the Mendeleev Ridge that have a very similar stratigraphy with HLY0503-8JPC (Fig. 4) (Polyak et al., 2004) for correlation with the Lomonosov Ridge core 96/12-1PC (Jakobsson et al., 2001). Some of the species occur only at certain stratigraphic intervals at both sites as well as in cores from other areas of the central Arctic Ocean with comparable water depths (Fig. 5) (Poore et al., 1994; Ishman et al., 1996; Nørgaard-Pedersen et al., 2007). Notably, *E. exigua*, a phytodetritus feeding foraminifer is absent from the Arctic today except in the seasonally ice-free area adjacent to the Fram Strait (Polyak, 1990; Wollenburg and Mackensen, 1998), but consistently occurs on the Lomonosov, Mendeleev, and Northwind ridges at the stratigraphic level now correlated to the bottom of MIS 5 (Poore et al., 1994; Jakobsson et al., 2001; Polyak et al., 2004). Another 'anomalous' assemblage has a high percentage of *B. aculeata* that prefers sediment with a fairly high amount of organic matter and/or oxygen deficiency (Lutze and Coulbourn, 1984; Mackensen et al., 1995).

The correlation with the central Lomonosov Ridge record allowed us to import the MIS scale substantiated for this site to HLY0503-8JPC where boundaries between major brown and grayish units (Fig. 2) are considered as glacial-interglacial (stadial-interstadial) transitions (Fig. 5). Identification of MIS 5 limits was aided by the position of subpolar planktonic peaks in HLY0503-8JPC and correlative occurrence of *B. aculeata* and *E. exigua* (Figs. 4 and 5). These planktonic and benthic indicators of low-ice conditions likely mark warm intervals and were attributed to MIS 5e and 5a in the GreenICE cores (Nørgaard-Pedersen et al., 2007). However, the position of the subpolar foraminiferal peaks may not exactly correspond to the boundaries of these stages. For example, the last-interglacial warming started ca. 5–6 kyr prior to the initiation of MIS 5 of 130 ka (e.g., CAPE,

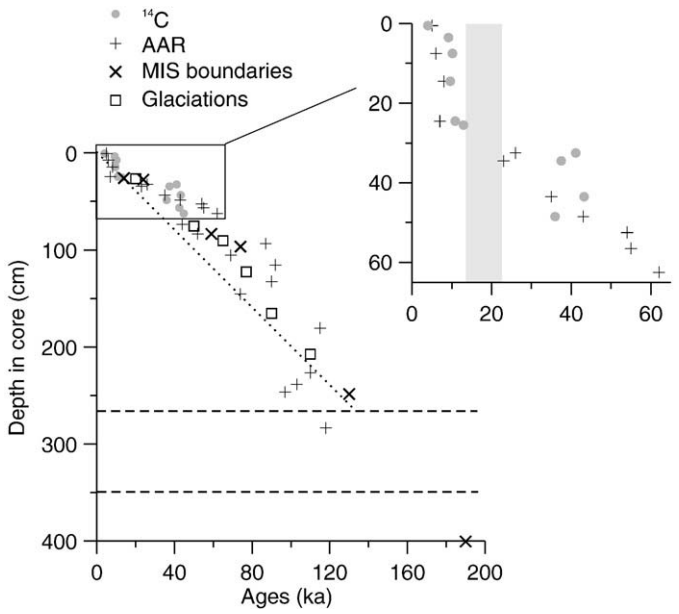

Fig. 6. Age-depth distribution in HLY0503-8JPC based on ^{14}C, amino acid racemization (AAR) (Kaufman et al., 2008), correlated Marine Isotopic Stage (MIS) boundaries and mid-points of glacial events (see Fig. 5 for correlations). Dashed lines bound the slump interval. Dotted line shows the 2 cm/kyr sedimentation rate slope. An enlarged upper part of the core details the last stadial cycle, with the LGM hiatus highlighted by shading.

2006). This offset is consistent with a seemingly early development of the lower subpolar peak in our data, which appears to start in MIS 6 by lithostratigraphic criteria (Fig. 5).

The elevated sedimentation rates in HLY0503-8JPC allow for a discrimination of cooling events with low foraminiferal abundance within the warm intervals, notably the carbonaceous debris layer interrupting MIS 5e at 230–235 cm and a gray, glacial-type unit within MIS 5a at 120–130 cm. Both events co-occur with pronounced δ^{18}O depletions and clearly represent massive discharges of icebergs and/or meltwater due to prolonged decay of large ice sheets. The latter event has been identified in a well-resolved sedimentary record from the eastern Arctic Ocean (Barents Sea slope) and interpreted as an outburst of an ice-dammed lake in northern Siberia around ca. 77 ka (Knies and Vogt, 2003).

In addition to correlations with the central Lomonosov Ridge, we tentatively correlate glacial intervals to major glaciations at the Eurasian Arctic margin with relatively well-constrained chronology (Svendsen et al., 2004; Larsen et al., 2006) along the lines suggested by Spielhagen et al. (2004). In particular, the two closely timed Middle Weichselian glaciations at ca. 60–70 ka (MIS 4) and 45–55 ka appear to match the grayish, mostly foraminiferal-barren HLY0503-8JPC unit between 70–100 cm with two pronounced sand spikes separated by a muted interstadial indicated by relatively high stable-isotopic values around 80 cm (Fig. 2). The upper boundary of this double-glacial unit corresponds to a marked interstadial onset dated to ca. 45–50 ka. Another extended grayish unit below ca. 250 cm correlates to MIS 6, which was the largest glaciation in northern Eurasia. We note however that the interval between ca. 270–350 cm is a slump, which was likely emplaced instantaneously and should be excluded from the age-depth estimates. Sedimentation on the Mendeleev Ridge has also been affected by glaciations in North America, as indicated for example by detrital carbonate layers, but in the deficiency of pre-LGM stratigraphic constraint for the northern Laurentide margin we use only the Eurasian glacial stratigraphy for now.

5.4. Sedimentation rates

The combination of these correlations with ^{14}C and AAR ages gives a consistent pattern of age-depth distribution for HLY0503-8JPC (Fig. 6). The average sedimentation rate through MIS 5 in this record is ~2 cm/kyr, which is ~20% lower than sedimentation rates estimated for the correlative portion of the ACEX record, but higher than in any other published record from the central Arctic Ocean with a constrained stratigraphy. Rates estimated for MIS 6-7 (without the slump interval) appear to be lower, but the age model for this part of the core is more tentative. Lower average rates for these ages may be partly related to a large hiatus during the MIS 6 glaciation, which was possibly the most extensive glaciation in the Arctic (e.g., Jakobsson et al., 2008a,b; Colleoni et al., 2009-this issue). Elevated sedimentation rates in HLY0503-8JPC in comparison with sites upslope on the Mendeleev Ridge (Fig. 4) probably reflect resuspension of fines at shallower depth and deposition at the slope foot; this interpretation, consistent with observations on nepheloid layers (Hunkins et al., 1969), indicates the role of bottom currents in this part of the Arctic Ocean. Samples taken from HLY0503-8JPC at 1 cm interval down at least to the bottom of MIS 5 provide an average resolution of 500 years per sample. However, sedimentation rates are not evenly distributed along the entire record, as revealed in the upper part of the core that has a more detailed age framework (Fig. 6). Highest rates, in excess of 10 cm/kyr, characterize deglacial and some interglacial/interstadial environments (such as in MIS 3 and the early Holocene), while the LGM is represented by a hiatus or nearly so. We infer that other glacial maxima likely contain similar hiatuses.

6. Discussion

6.1. Sedimentary and hydrographic environments

The sedimentary cycles we see in HLY0503-8JPC have been generally interpreted for the correlative sediments in the central Arctic Ocean including the Mendeleev Ridge (Polyak, 1986; Darby et al., 1997; Poore et al., 1999; Polyak et al., 2004), but a higher resolution and more comprehensive age control for HLY0503-8JPC allow for a deeper and more detailed understanding of paleoceanographic environments. To assist the interpretation of observed proxy records, we have plotted the most informative proxies vs. age (Fig. 7) using the correlation tie points as discussed above and ^{14}C ages above the LGM.

Brown, faunal-rich units, including the surficial Holocene interval, occur during interglacial-type periods characterized by diminished ice sheets and high sea levels (e.g., Darby et al., 2006). It has been shown that brown sediment color in the Arctic Ocean is caused by high Mn hydroxide contents, possibly resulting from enhanced oxidation of the sediment surface and/or higher riverine fluxes from the Eurasian margin (Jakobsson et al., 2000; Polyak et al., 2004; O'Regan et al., 2008). Yet another possibility is that Mn precipitation is biologically mediated and therefore related to changes in productivity (e.g., Gebhardt et al., 2005). Regardless of the exact nature of the underlying processes, a high concurrent biogenic component suggests higher productivity and thus, lower ice conditions during the deposition of brown sediment. This interpretation helps explain variability in δ^{13}C between brown and grayish units in relationship with ice-cover conditions, where more solid ice is likely to decrease air-sea gas exchange and thus, δ^{13}C values in DIC. The occurrence of moderate levels of detrital sand including coarser grains at some intervals indicate the role of sea-ice sediment transport during interglacial/interstadial periods.

Grayish units signify very different environments of glacial-type periods when the Arctic Ocean was impacted by vast inputs of icebergs and meltwater from surrounding ice sheets, continental margins were either exposed or covered by ice, and the exchange of water masses with other oceans was limited (e.g., Darby et al., 2006). These units have little, if any, accumulation of biological material, probably related to some combination of thicker and more solid ice cover, common meltwater pulses, and lack of food supply from the margins. Fine, muddy sediment

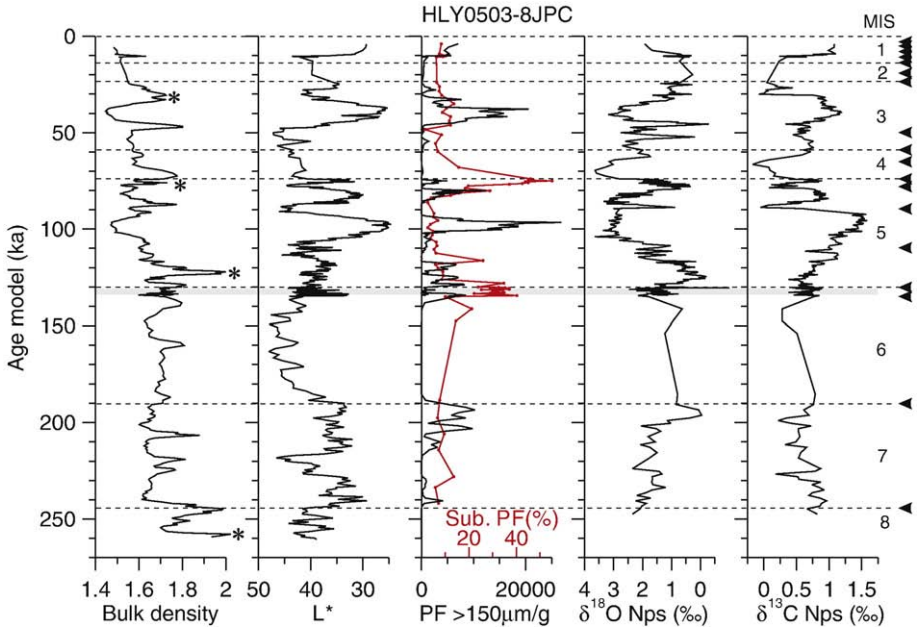

Fig. 7. Distribution of proxies in HLY0503-8JPC vs. age. Arrowheads on the right indicate age tie points based on correlations explained in Fig. 5 and accompanying text, plus ^{14}C ages above the LGM. Subpolar planktonic foraminiferal content (75–150 μm) is shown by gray line in the same panel with foraminiferal abundance. Detrital carbonate layers are shown by stars. Slump interval in the upper part of MIS 6 is shaded.

in the central part of some glacial units suggests negligible contribution from ice rafting, probably due to the solidly ice-bound ocean surface, be it an ice shelf (Polyak et al., 2001; Jakobsson et al., 2008b) or thickened sea ice (Bradley and England, 2008; Polyak et al., 2009-this issue). We suggest that the major source of this sediment was glacial flour delivered by meltwater from ice-sheet margins at the Arctic Ocean periphery. This sediment type is characteristic of glacial units in the western Arctic Ocean, but does not appear to be common in the Eurasian Basin including the Lomonosov Ridge, where correlative units mostly have high sand content (Jakobsson et al., 2001; Spielhagen et al., 2004). This distribution possibly marks the limits of the solid ice cover, which may have caused hiatuses in the central part of the ocean, as exemplified by the conspicuous hiatus during the LGM observed in many sediment cores from the western Arctic Ocean (Polyak et al., 2009-this issue).

Glacial terminations and inception episodes are characterized by pronounced sand and coarser-grain spikes (Figs. 2 and 7), most likely due to the influx of large numbers of icebergs into the basin during periods of ice-sheet instability. Some of these spikes have recognizable petrographic compositions, notably the pinkish/whitish layers of detrital carbonates indicative of Canadian Arctic provenance (Darby, 1971; Bischof et al., 1996; Phillips and Grantz, 2001). The two largest detrital carbonate peaks with numerous coarse clasts are located near glacial terminations of MIS 8 and MIS 6 and are correlated to PW (pink-white) layers 1 and 2 in D. Clark's stratigraphy (Clark et al., 1980); notable concentrations of carbonate debris also occur in late MIS 5a and MIS 3. These layers are especially well expressed in areas closer to the Laurentide margin such as the Northwind Ridge, but can be traced all the way through the western Arctic Ocean, which makes them excellent stratigraphic markers (Polyak et al., 2009-this issue). In contrast, some of the sand spikes, identified notably in HLY0503-8JPC in MIS 4 and mid-MIS 3 as well as near the top of MIS 6 and MIS 8, are composed primarily of quartz grains and are likely related to Eurasian sources (Polyak et al., 2004). This provenance indicates that circulation during some glacial periods may have been different from the present Beaufort Gyre dominated system in the western Arctic Ocean. Another possible explanation for the Eurasian glacial material on the Mendeleev Ridge implies the existence of sizeable ice sheets at the eastern Eurasian margin such as on the East-Siberian shelf (Grosswald, 1980; Tumskoy and Basilyan, 2007).

The gravity flow or slump deposit in the upper part of MIS 6 may be related to the grounding of large ice masses (ice rise) on the southernmost part of the Mendeleev Ridge; seafloor traces of this ice grounding have been mapped on the 2008 Polarstern cruise (W. Jokat, pers. comm., 2008). Multiple lines of evidence show that MIS 6 was possibly the largest circum-Arctic glaciation, when glacier ice of several hundred meters thick extended deep in the interior of the Arctic Ocean (Jakobsson et al., 2008b and references therein). The findings suggesting that the Mendeleev Ridge was also affected by these glacier expansions gives additional weight to the premise that large ice sheets existed on the East-Siberian shelf.

Grayish units are also characterized by spikes of especially low $\delta^{18}O$ composition (to −0.5‰), mostly associated with sandy layers, but also occurring in some fine-grained intervals such as in early MIS 3 (Figs. 2 and 7). These pronounced $\delta^{18}O$ depletions, typically accompanied by low $\delta^{13}C$ values, are indicative of voluminous, pulsed meltwater discharges as documented throughout the Arctic Ocean (e.g., Stein et al., 1994; Poore et al., 1999; Spielhagen et al., 2004, 2005; Knies et al., 2007). These events were probably related to the drainage of large proglacial lakes such as those mapped along the southern margin of Eurasian ice sheets (Mangerud et al., 2004) or subglacial reservoirs, the importance of which is increasingly recognized for both modern and past ice sheets (Bell et al., 2007; Anderson and Fretwell, 2008; Lajeunesse and St-Onge, 2008). The source of these meltwater events cannot be reconstructed from stable-isotope records alone and require additional provenance proxies. For example, based on the elevated Ba/Ca ratios in Nps from the post-LGM $\delta^{18}O$ depletion spikes in the Mendeleev Ridge cores, these events were attributed to meltwater originating from the Laurentide ice sheet (Hall and Chan, 2004). This interpretation is corroborated by the elevated amounts of detrital carbonates and iron-oxide grains with Laurentide provenance in this part of the Mendeleev Ridge stratigraphy (Darby et al., 2002; Polyak et al., 2004). In contrast, $\delta^{18}O$ minimum in the previous glacial unit corresponding to the penultimate (mid-MIS 3) Eurasian glaciation is associated with non-carbonaceous sand, which indicates the likely Eurasian origin.

One notable exception to the prevailing downcore stable-isotopic pattern, where changes in $\delta^{18}O$ typically co-vary with $\delta^{13}C$, is the co-occurrence of high $\delta^{18}O$ with low $\delta^{13}C$ values in MIS4 (Fig. 7). This anomaly has been tentatively explained for GreenICE cores by the contamination of foraminiferal tests by fine-grained detrital carbonate (Nørgaard-Pedersen et al., 2007). However, the wide geographic distribution of this event (see also Spielhagen et al., 2004) and the lack of detrital carbonates in this layer in western Arctic cores requires a different interpretation. We propose that this unusual stable-isotopic signature is related to the actual glacial-maximum environment with little meltwater in the basin. The reason why such an environment is not found in MIS 2 and 6 may be caused by hiatuses in place of glacial culminations.

6.2. Paleoclimatic implications

The developed age model was used for evaluating the spectral distribution of downcore changes. We have chosen L* as a continuously measured parameter that has a distribution similar to foraminiferal abundance and $\delta^{13}C$ in the investigated record (Figs. 2 and 7), and thus presumably approximates biological production and ice conditions. The application of the Blackman–Tukey method to the L* time series resulted in two distinct power frequencies around 0.01 and 0.05, which correspond to the 100-kyr and precessional (19–20 kyr) cycles, respectively (Fig. 8). The use of bulk density, a continuously measured series related to glacial inputs and somewhat similar to the $\delta^{18}O$ record, did not produce any meaningful spectral pattern (not shown), indicating a noisier signal. The 100-kyr cycle apparent in the L* time series may not be evaluated with confidence in a record of only 260-kyr long, but this result is consistent with the longer-term variability in the ACEX record that shows a clearly recognizable 100-kyr cyclicity in the Middle to Late Quaternary, beginning ca. 1 Ma (O'Regan et al., 2008). Furthermore, the ACEX spectral record shows a potentially strong precessional control, especially in early Pleistocene sediments. The precessional control is commonly associated with low-latitude processes (e.g., Braconnot and Marti, 2003), but the Arctic also has a potential for its amplification through changes in sea-ice and snow albedo and the poleward transport of heat and moisture (Jackson and Broccoli, 2003; Khodri et al., 2005). These precession-driven mechanisms may have affected sea-ice conditions and the formation of ice sheets at the Arctic periphery, which possibly interacted with 100-kyr glacial cycles to produce the pattern observed in HLY0503-8JPC, further complicated by threshold events such as glacial surges and pro/subglacial drainage pulses. More investigation is needed to understand the spectral distribution and underlying mechanisms in Arctic paleoceanographic records; in particular, the apparently diminutive obliquity signal requires explanation.

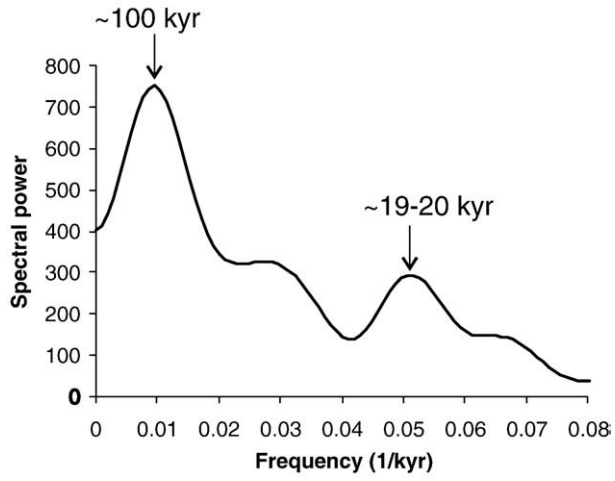

Fig. 8. Power spectra of L* series in HLY0503-8JPC (see Fig. 7 for plot vs. age; slump interval removed) generated using the Blackman–Tukey method with 80% confidence interval (AnalySeries 1.1).

One important question today is what was the Arctic Ocean like during full interglacial times, which may provide a close analog for the expected future conditions. The high content of subpolar planktonic foraminifers in the intervals corresponding to MIS 5a and 5e (starting possibly somewhat earlier than MIS 5e proper) in HLY0503-8JPC (Figs. 4 and 7) and GreenICE cores suggests low-ice, probably seasonally ice-free conditions. Based on the modern distribution of planktonic foraminifers in the Norwegian-Greenland Sea (e.g., Johannessen et al., 1994), we infer that high numbers of *N. incompta* at some levels in the correlative intervals in HLY0503-8JPC indicate even more open-ice conditions than in the GreenICE area. We note that subpolar planktonic foraminifers in the Arctic Ocean have small test sizes, and therefore may have been overlooked in many studies that used size fractions >150 or >125 μm. The MIS 5e and 5a intervals are also characterized by the presence of benthic foraminifers *E. exigua* and *B. aculeata*, respectively (Figs. 4 and 5), indicative of higher productivity and thus, the proximity of the sea-ice margin. These results imply that low-ice conditions were widespread in the Arctic Ocean during the last interglacial and, with some variation, in MIS 5a. In contrast, Holocene sediments do not have apparent low-ice indications in foraminiferal faunas — neither in HLY0503-8JPC, nor in GreenICE; whereas, proxy records from the Holocene in the Norwegian–Greenland Sea indicate more northern extension of warm waters than in the last interglacial (e.g., Bauch and Erlenkeuser, 2008). Understanding the reasons for different responses of the Arctic Ocean to warming during different interglacials is critical for predicting the future changes in the Arctic system.

It is also interesting that the stable isotope values as well as foraminiferal abundance and brown color intensity in the central Arctic cores are not as high in MIS 5e, as would be expected for a full interglacial, which might be explained by an enhanced stratification of the water column. One possible explanation is the lag effect of MIS 6 ice sheets, which may have released large amounts of meltwater into the central Arctic Ocean after the onset of interglacial conditions. A similar pattern has been inferred for the early phase of MIS 5e in the Norwegian–Greenland Sea (Bauch and Erlenkeuser, 2008). Although the last interglacial at the northern Eurasian margin is generally marked by fairly warm-water fauna (e.g., Funder et al., 2002), the deglaciation history is not well constrained; even less is known about the MIS 6 ice-sheet limits and deglaciation in North America. The other possibility is that high stratification of the Arctic Ocean during the interglacial was due to melting sea ice and higher precipitation/runoff levels. If this is the case, we can expect similar environments in the Arctic in the near future with sea-ice retreat and an increase in runoff (Holland et al., 2006; Min et al., 2008).

7. Summary

The investigation of the upper 5 m in core HLY0503-8JPC from the base of the eastern flank of the Mendeleev Ridge allows for the reconstruction of the paleoceanographic evolution in this part of the Arctic Ocean for the last ca. 250 kyr (MIS 1 to 7). The estimated average sampling resolution is 0.5 kyr at least for the Late Quaternary interval embracing the last full glacial cycle and the last interglacial (MIS 5e). This study confirms earlier conclusions on strongly contrasting sedimentary environments in the western Arctic Ocean between interglacial-type and glacial-type periods (e.g., Phillips and Grantz, 1997; Polyak et al., 2004), and allows these variations to be placed into an updated chronostratigraphic framework, and thus into a global paleoclimatic context.

Interglacial-type intervals including the Holocene are primarily characterized by moderate to low sea ice conditions, enhanced biological productivity, and sedimentation from ice rafting and

possibly deep currents. Glacial intervals differed by stronger stratification of the water column and presumably very solid ice cover that suppressed both biological life and pelagic sedimentation, with episodes of massive iceberg discharges from glaciated Arctic margins during glacial inceptions and terminations. The periodicity of these variations appears to combine 100-kyr and precessional Milankovich time scales, possibly reflecting interaction of insolation-controlled processes with longer-term glacial cycles. Superimposed on this pattern are abrupt iceberg- and/or meltwater-discharge events with provenance indicative of both Laurentide and Eurasian sources.

The interval identified as the last interglacial (MIS 5e), as well as MIS 5a, features anomalous planktonic and benthic foraminiferal assemblages indicative of strongly reduced sea-ice cover. The interglacial interval also differs from younger interstadials by proxy indications of enhanced stratification, which might be related to warmer climate and higher precipitation or to the lag effect of the MIS 6 mega-glaciation. These results are especially important in the context of the present-day shrinkage of the Arctic sea ice and the necessity to predict the consequences of this change for future environments.

Acknowledgments

HOTRAX'05 coring expedition and this post-cruise research were supported by the US NSF-OPP awards ARC-0352359/0352395 and ARC-0612473. We thank the HOTRAX'05 team for help with collection and processing of the HLY0503 cores, and Yohei Matsui for assistance with stable-isotope analyses. J. Matthiessen and an anonymous reviewer provided insightful comments.

References

Aagaard, K., Swift, J., Carmack, E., 1985. Thermohaline circulation in the Arctic Mediterranean seas. J. Geophys. Res. 90, 4833–4846.
Anderson, J.B., Fretwell, L.O., 2008. Geomorphology of the onset area of a paleo-ice stream, Marguerite Bay, Antarctic Peninsula. Earth Surf. Processes Landf. 33, 503–512.
Andreeva, I.A., Basov, V.A., Kupriyanova, N.V., Shilov, V.V., 2007. Age and depositional environments of bottom sediments in the Mendeleev Ridge area, Arctic Ocean [Vozrast i usloviya formirovaniya donnyh osadkov v raione podnyatiya Mendeleeva (SLO)]. Trans. [Trudy] NIIGA – VNIIOkeangeologiya 211, 131–150 (in Russian).
Backman, J., Jakobsson, M., Løvlie, R., Polyak, L., Febo, L.A., 2004. Is the central Arctic Ocean a sediment starved basin? Quat. Sci. Rev. 23, 1435–1454.
Bauch, A.H., Erlenkeuser, H., 2008. A "critical" climatic evaluation of last interglacial (MIS 5e) records from the Norwegian Sea. Polar Res. 27, 131–151.
Bauch, D., Carstens, J., Wefer, G., 1997. Oxygen isotope composition of living *Neogloboquadrina pachyderma* (sin.) in the Arctic Ocean. Earth Planet. Sci. Lett. 146, 47–58.
Bauch, D., Carstens, J., Wefer, G., Thiede, J., 2000. The imprint of anthropogenic CO_2 in the Arctic Ocean: evidence from planktic $\delta^{13}C$ data from water column and sediment surfaces. Deep-Sea Res. II 47, 1791–1808.
Bell, R.E., Studinger, M., Shuman, C.A., Fahnestock, M.A., Joughin, I., 2007. Large subglacial lakes in East Antarctica at the onset of fast-flowing ice streams. Nature 445, 904–907.
Bischof, J., Clark, D., Vincent, J., 1996. Pleistocene paleoceanography of the central Arctic Ocean: the sources of ice rafted debris and the compressed sedimentary record. Paleoceanography 11, 743–756.
Braconnot, P., Marti, O., 2003. Impact of precession on monsoon characteristics from coupled ocean atmosphere experiments: changes in Indian monsoon and Indian ocean climatology. Mar. Geol. 201, 23–34.
Bradley, R.S., England, J.H., 2008. The Younger Dryas and the sea of ancient ice. Quat. Res. 70, 1–10.
CAPE-Last Interglacial Project Members, 2006. Last Interglacial Arctic warmth confirms polar amplification of climate change. Quat. Sci. Rev. 25, 1383–1400.
Carter, R.M., 1975. A discussion and classification of subaqueous mass-transport with particular application to gravity flow, slurry flow and fluxoturbidites. Earth-Sci. Rev. 11, 145–177.
Clark, D.L., Whitman, R.R., Morgan, K.A., Mackey, S.D., 1980. Stratigraphy and glacial marine sediments of the Amerasian Basin, central Arctic Ocean. Geol. Soc. Amer. Spec. Paper 181, 57.
Clark, D.L., Chern, L.A., Hogler, J.A., Mennicke, C.M., Atkins, E.D., 1990. Late Neogene climatic evolution of the central Arctic Ocean. Mar. Geol. 93, 69–94.
Clough, L., Ambrose Jr., W., Cochran, K., Barnes, C., Renaud, P., Aller, R., 1997. Infaunal density, biomass and bioturbation in the sediments of the Arctic Ocean. Deep-Sea Res. II 44, 1683–1704.
Colleoni, F., Krinner, G., Jakobsson, M., Peyaud, V., Ritz, C., 2009. Influence of regional parameters on the surface mass balance of the Eurasian ice sheet during the peak Saalian (140 kya). Glob. Planet. Change 68, 132–148 (this issue).
Comiso, J.C., Parkinson, C.L., Gersten, R., Stock, L., 2008. Accelerated decline in the Arctic sea ice cover. Geophys. Res. Lett. 35, L01703.
Cronin, T.M., Smith, S., Eynaud, F., O'Regan, M., King, J., 2008. Quaternary paleoceanography of the central Arctic based on Integrated Ocean Drilling Program Arctic Coring Expedition 302 foraminiferal assemblages. Paleoceanography 23, PA1S18.
Darby, D.A., 1971. Carbonate cycles and clay mineralogy of Arctic Ocean sediment cores. Ph.D. Thesis, Univ. Wisconsin-Madison, 43 p.
Darby, D.A., Bischof, J.F., Jones, G.A., 1997. Radiocarbon chronology of depositional regimes in the western Arctic Ocean. Deep-Sea Res. 44, 1745–1757.
Darby, D., Bischof, J., Spielhagen, R., Marshal, S., Herman, S., 2002. Arctic ice export events and their potential impact on global climate during the late Pleistocene. Paleoceanography 17 15–1 to 15–17.
Darby, D., Jakobsson, M., Polyak, L., 2005. Icebreaker expedition collects key Arctic seafloor and ice data. EOS 86, 549–556 No. 52.
Darby, D.A., Polyak, L., Bauch, H., 2006. Past glacial and interglacial conditions in the Arctic Ocean and marginal seas — a review. In: Wassman, P. (Ed.), Structure and function of contemporary food webs on Arctic shelves: a Pan-Arctic comparison: Progr. Oceanography, vol. 71, pp. 129–144.
Dyke, A.S., Andrews, J.T., Clark, P.U., England, J.H., Miller, G.H., Shaw, J., Veillette, J.J., 2002. The Laurentide and Innuitian ice sheets during the Last Glacial maximum. Quat. Sci. Rev. 21, 9–31.
Fahl, K., Nöthig, E.M., 2007. Lithogenic and biogenic particle fluxes on the Lomonosov Ridge (central Arctic Ocean) and their relevance for sediment accumulation: vertical vs. lateral transport. Deep-Sea Res. I 54, 1256–1272.
Fairbanks, R.G., Mortlock, R.A., Chiu, T.-C., Cao, L., Kaplan, A., Guilderson, T.P., Fairbanks, T.W., Bloom, A.L., 2005. Marine radiocarbon calibration curve spanning 0 to 50,000 years B.P. based on paired 230Th/234U/238U and 14C dates on pristine corals. Quatern. Sci. Rev. 24, 1781–1796.
Funder, S., Demidov, I., Yelovicheva, Y., 2002. Hydrography and mollusc faunas of the Baltic and the White Sea-North Sea seaway in the Eemian. Palaeogeogr. Palaeoclimatol. Palaeoecol. 184, 275–304.
Gebhardt, A.C., Schoster, F., Gaye-Haake, B., Beeskow, B., Rachold, V., Unger, D., Ittekkot, V., 2005. The turbidity maximum zone of the Yenisei River (Siberia) and its impact on organic and inorganic proxies. Estuar. Coast. Shelf Sci. 65, 61–73.
Glasby, G.P., 2006. Manganese: predominant role of nodules and crusts, In: Schulz, H.D., Zabel, M. (Eds.), Marine geochemistry, 2nd edition. Springer, Berlin, Heidelberg, pp. 371–427.
Goodfriend, G.A., Brigham-Grette, J., Miller, G.H., 1996. Enhanced age resolution of the marine Quaternary record in the Arctic using aspartic acid racemization dating of bivalve shells. Quat. Res. 45, 176–187.
Gosselin, M., Levasseur, M., Wheeler, P., Horner, R., Booth, B., 1997. New measurements of phytoplankton and ice algal production in the Arctic Ocean. Deep-Sea Res. II 44, 1623–1644.
Grosswald, M.G., 1980. Late Weichselian ice sheets of northern Eurasia. Quat. Res. 13, 1–32.
Hall, J.M., Chan, L.H., 2004. Ba/Ca in benthic foraminifera; thermocline and middepth circulation in the North Atlantic during the last glaciation. Paleoceanography 19, PA1017.
Hillaire-Marcel, C., de Vernal, A., Polyak, L., Darby, D., 2004. Size-dependent isotopic composition of planktic foraminifers from Chukchi Sea vs. NW Atlantic sediments — implications for the Holocene paleoceanography of the western Arctic. Quat. Sci. Rev. 23, 245–260.
Holland, M.M., Finnis, J., Serreze, M.C., 2006. Simulated Arctic Ocean freshwater budgets in the twentieth and twenty-first centuries. J. Climate 19, 6221–6242.
Hunkins, K., Thorndike, E.M., Mathieu, G., 1969. Nepheloid layers and bottom currents in the Arctic Ocean. J. Geophys. Res. 74, 6995–7008.
Ishman, S., Polyak, L., Poore, R., 1996. An expanded record of Pleistocene deep Arctic change: Canada Basin, western Arctic Ocean. Geology 24, 139–142.
Jackson, S.C., Broccoli, A.J., 2003. Orbital forcing of Arctic climate: mechanisms of climate response and implications for continental glaciation. Clim. Dyn. 21, 539–557.
Jackson, H.R., Mudie, P.J., Blasco, S.M. (Eds.), 1985. Initial geological report on CESAR – the Canadian expedition to study the Alpha Ridge, Arctic Ocean: Geol. Survey Canada Paper, pp. 22–84. 177 pp.
Jakobsson, M., Løvlie, R., Al-Hanbali, H., Arnold, E., Backman, J., Mörth, M., 2000. Manganese color cycles in Arctic Ocean sediments constrain Pleistocene chronology. Geology 28, 23–26.
Jakobsson, M., Løvlie, R., Arnold, E., Backman, J., Polyak, L., Knutsen, J., Musatov, E., 2001. Pleistocene stratigraphy and paleoenvironmental variation from Lomonosov Ridge sediments, central Arctic Ocean. Glob. Planet. Change 31, 1–21.
Jakobsson, M., Macnab, R., Mayer, L., Anderson, R., Edwards, M., Hatzky, J., Schenke, H.W., Johnson, P., 2008a. An improved bathymetric portrayal of the Arctic Ocean: implications for ocean modeling and geological, geophysical and oceanographic analyses. Geophys. Res. Let. 35, L07602.
Jakobsson, M., Polyak, L., Edwards, M.H., Kleman, J., Coakley, B.J., 2008b. Glacial geomorphology of the central Arctic Ocean: Chukchi Borderland and the Lomonosov Ridge. Earth Surf. Processes Landf. 33, 526–545.
Johannessen, T., Jansen, E., Flatoy, A., Ravelo, A.C., 1994. The relationship between surface water masses, oceanographic fronts and paleoclimatic proxies in surface sediments of the Greenland, Iceland, Norwegian seas. In: NATO ASI Series, vol. 117. Springer, Berlin, Heidelberg, pp. 61–85.
Kaufman, D., Polyak, L., Adler, R., Channell, J., Xuan, C., 2008. Dating late Quaternary planktonic foraminifer *Neogloboquadrina pachyderma* from the Arctic Ocean by using amino acid racemization. Paleoceanography 23, PA3224.
Khodri, M., Cane, M.A., Kukla, G., Gavin, J., Braconnot, P., 2005. The impact of precession changes on the Arctic climate during the last interglacial–glacial transition. Earth Planet. Sci. Lett. 236, 285–304.
Kirschvink, J.L., 1980. The least squares lines and plane analysis of paleomagnetic data. Geophys. J. R. Astron. Soc. 62, 699–718.
Knies, J., Vogt, C., 2003. Freshwater pulses in the eastern Arctic Ocean during Saalian and Early Weichselian ice-sheet collapse. Quat. Res. 60, 243–251.

Knies, J., Matthiessen, J., Mackensen, A., Stein, R., Vogt, C., Frederichs, T., Num, S., 2007. Effects of Arctic freshwater forcing on thermohaline circulation during the Pleistocene. Geology 35, 1075–1078.
Lajeunesse, P., St-Onge, G., 2008. The subglacial origin of the Lake Agassiz–Ojibway final outburst flood. Nat. Geosci. 1, 184–188.
Larsen, E., Kjær, K.H., Demidov, I.N., Funder, S., Grøsfjeld, K., Houmark-Nielsen, M., Jensen, M., Linge, H., Lysa, A., 2006. Late Pleistocene glacial and lake history of northwestern Russia. Boreas 35, 394–424.
Lutze, G.F., Coulbourn, W.T., 1984. Recent benthic foraminifera from the continental margin of northwest Africa: community structure and distribution. Mar. Micropaleontol. 8, 361–401.
Mackensen, A., Schmiedl, G., Harloff, J., Giese, M., 1995. Deep-sea foraminifera in the South Atlantic Ocean: ecology and assemblage generation. Micropaleontology 41, 342–358.
Mangerud, J., Jakobsson, M., Alexanderson, H., Astakhov, V., Clarke, G.K.C., Henriksen, M., Hjort, C., Krinner, G., Lunkka, J.P., Möller, P., Murray, A., Nikolskaya, O., Saarnisto, M., Svendsen, J.I., 2004. Ice-dammed lakes and rerouting of the drainage of northern Eurasia during the last glaciation. Quat. Sci. Rev. 23, 1313–1332.
Martinson, D.G., Pisias, N.G., Hays, J.D., Imbrie, J., Moore, T.C., Shackleton, N.J., 1987. Age dating and the orbital theory of the ice ages — development of a high-resolution 0 to 300,000-year chronostratigraphy. Quat. Res. 27, 1–29.
Middleton, G.V., Hampton, M.A., 1976. Subaqueous sediment transport and deposition by sediment gravity flows. In: Stanley, D.J., Swift, D.J.P. (Eds.), Marine Sediment Transport and Environmental Management. In: Wiley, New York, pp. 197–218.
Min, S.K., Zhang, X., Zwiers, F., 2008. Human-induced Arctic moistening. Science 320, 518–520.
Nørgaard-Pedersen, N., Spielhagen, R., Thiede, J., Kassens, H., 1998. Central Arctic surface ocean environment during the past 80,000 years. Paleoceanography 13, 193–204.
Nørgaard-Pedersen, N., Mikkelsen, N., Kristoffersen, Y., 2007. Arctic Ocean record of last two glacial-interglacial cycles off North Greenland/Ellesmere Island — implications for glacial history. Mar. Geol. 244, 93–108.
O'Regan, M., King, J., Backman, J., Jakobsson, M., Pälike, H., Moran, K., Heil, C., Sakamoto, T., Cronin, M., Jordan, R., 2008. Constraints on the Pleistocene chronology of sediments from the Lomonosov Ridge. Paleoceanography 23, PA1S19.
Otto-Bliesner, B.L., Marshall, S.J., Overpeck, J.T., Miller, G.H., Hu, A., C.L.I. members, 2006. Simulating Arctic climate warmth and icefield retreat in the last interglaciation. Science 311, 1751–1753.
Phillips, R., Grantz, A., 1997. Quaternary history of sea ice and paleoclimate in the Amerasia basin, Arctic Ocean, as recorded in the cyclical strata of Northwind Ridge. Geol. Soc. Amer. Bull. 109, 1101–1115.
Phillips, R.L., Grantz, A., 2001. Regional variations in provenance and abundance of ice-rafted clasts in Arctic Ocean sediments: implications for the configuration of late Quaternary oceanic and atmospheric circulation in the Arctic. Mar. Geol. 172, 91–115.
Polyak, L.V., 1986. New data on microfauna and stratigraphy of bottom sediments of the Mendeleev Ridge, Arctic Ocean. In: Andreev, S.I. (Ed.), Sedimentogenes i konkrecioobrazovanie v okeane (Sedimentogenesis and nodule-formation in the Ocean). InSevmorgeologia, Leningrad, pp. 40–50 (in Russian).
Polyak, L.V., 1990. General trends of benthic foraminiferal distribution in the Arctic Ocean. In: Kotlyakov, V.M., Sokolov, V.E. (Eds.), Arctic Research: Advances and Prospects. Part 2. InNauka, Moscow, pp. 211–213.
Polyak, L., Edwards, M.H., Coakley, B.J., Jakobsson, M., 2001. Ice shelves in the Pleistocene Arctic Ocean inferred from glaciogenic deep-sea bedforms. Nature 410, 453–457.
Polyak, L., Curry, W.B., Darby, D.A., Bischof, J., Cronin, T.M., 2004. Contrasting glacial/interglacial regimes in the western Arctic Ocean as exemplified by a sedimentary record from the Mendeleev Ridge. Palaeogeogr. Palaeoclimatol. Palaeoecol. 203, 73–93.
Polyak, L., Bischof, J., Ortiz, J., Darby, D., Channell, J., Xuan, C., Kaufman, D., Lovlie, R., Schneider, D., Adler, R., 2009. Late Quaternary stratigraphy and sedimentation patterns in the western Arctic Ocean. Glob. Planet. Change XREF:doi:10.1016/j.gloplacha.2009.03.014.
Poore, R., Phillips, L., Rieck, H., 1993. Paleoclimate record for Northwind Ridge, western Arctic Ocean. Paleoceanography 8, 149–159.
Poore, R., Ishman, S., Phillips, L., McNeil, D., 1994. Quaternary stratigraphy and paleoceanography of the Canada Basin, western Arctic Ocean. U.S. Geol. Surv. Bull. 2080, 32.
Poore, R., Osterman, L., Curry, W., Phillips, R., 1999. Late Pleistocene and Holocene meltwater events in the western Arctic Ocean. Geology 27, 759–762.
Rigor, I.G., Wallace, J.M., Colony, R.I., 2002. On the response of sea ice to the Arctic Oscillation. J. Climate 15, 2648–2668.
Rudels, B., Jones, E.P., Schauer, U., Eriksson, P., 2004. Atlantic sources of the Arctic Ocean surface and halocline waters. Polar Res. 23, 181–208.
Scott, D.B., Mudie, P.J., Baki, V., MacKinnon, K.D., Cole, F.E., 1989. Biostratigraphy and late Cenozoic paleoceanography of the Arctic Ocean: foraminiferal, lithostratigraphic, and isotopic evidence. Geol. Soc. Amer. Bull. 101, 260–277.
Sellen, E., Jakobsson, M., Backman, J., 2008. Sedimentary regimes in Arctic's Amerasian and Eurasian basins: clues to differences in sedimentation rates. Glob. Planet. Change 61, 275–284.
Spielhagen, R., Baumann, K., Erlenkeuser, H., Nowaczyk, N., Nørgaard-Pedersen, N., Vogt, C., Weiel, D., 2004. Arctic Ocean deep-sea record of northern Eurasian ice sheet history. Quat. Sci. Rev. 23, 1455–1483.
Spielhagen, R.F., Erlenkeuser, H., Siegert, C., 2005. History of freshwater runoff across the Laptev Sea (Arctic) during the last degaciation. Glob. Planet. Change 23, 1455–1483.
Stein, R., Nam, S.I., Schubert, C., Vogt, C., Fütterer, D., Heinemeier, J., 1994. The last deglaciation event in the eastern Central Artic Ocean. Science 264, 692–696.
Steuerwald, B.A., Clark, D.L., Andrew, J.A., 1968. Magnetic stratigraphy and faunal patterns in Arctic Ocean sediments. Earth Planet. Sci. Lett. 5, 79–85.
Svendsen, J.I., Alexanderson, H., Astakhov, V.I., Demidov, I., Dowdeswell, J.A., Funder, S., Gataullin, V., Henriksena, M., Hjort, C., Houmark-Nielsen, M., Hubberten, H.W., Olfsson, I., Jakobsson, M., Kjæri, K.H., Larsen, E., Lokrantz, H., Pekka Lunkka, J., Lysså, A., Mangeruda, J., Matiouchkov, A., Murray, A., Mölleri, P., Niessen, F., Nikolskaya, O., Polyak, L., Saarnisto, M., Siegert, M., Spielhagen, R.F., Stein, R., 2004. Late Quaternary ice sheet history of northern Eurasia. Quat. Sci. Rev. 23, 1229–1271.
Tumskoy, V., Basilyan, A., 2007. Geological, permafrost and glacial interactions in Siberian Arctic: an idea for an new international project. First Conference on Arctic Palaeoclimate and its Extremes: Planning of International Polar Year activities and preliminary results. In: Stockholm University, Royal Swedish Academy of Sciences, Stockholm, Sweden.
Volkmann, R., Mensch, M., 2001. Stable isotope composition ($\delta^{18}O$, $\delta^{13}C$) of living planktic foraminifers in the outer Laptev Sea and the Fram Strait. Mar. Micropaleontol. 42, 163–188.
Weber, M.E., Niessen, F., Kuhn, G., Wiedicke, M., 1997. Calibration and application of marine sedimentary physical properties using a multi-sensor core logger. Mar. Geol. 136, 151–172.
Wollenburg, J.E., Mackensen, A., 1998. Living benthic foraminifers from the central Arctic Ocean: faunal composition, standing stock and diversity. Mar. Micropaleontol. 34, 153–185.
Xuan, C., Channell, J.E., Polyak, L., 2008. Origin of apparent magnetic excursions in Arctic deep-sea sediments. Eos Trans. AGU 89 (53) Fall Meet. Suppl., Abstract GP21B-0784.
Yamamoto, M., Polyak, L., 2009. Changes in terrestrial organic matter input to the Mendeleev Ridge, western Arctic Ocean, during the Late Quaternary. Glob. Planet. Change 68, 30–37 (this issue).